ACS APPLIED MATERIALS & INTERFACES

Research Article

www.acsami.org

Porous Carbon Nanofibers from Electrospun Biomass Tar/Polyacrylonitrile/Silver Hybrids as Antimicrobial Materials

Kunlin Song,[†] Qinglin Wu,[*,§,†] Zhen Zhang,[†] Suxia Ren,[§] Tingzhou Lei,[*,§] Ioan I. Negulescu,[‡] and Quanguo Zhang[⊥]

[†]School of Renewable Natural Resources, Louisiana State University, Baton Rouge, Louisiana 70803, United States

[§]Key Biomass Energy Laboratory of Henan Province, Zhengzhou, Henan 450008, China

[‡]Department of Textiles, Apparel Design and Merchandising, Louisiana State University, Baton Rouge, Louisiana 70803, United States

[⊥]Collaborative Innovation Center of Biomass Energy of Henan Province, College of Mechanical and Electrical Engineering, Henan Agricultural University, Zhengzhou, Henan 450002, China

Supporting Information

ABSTRACT: A novel route to fabricate low-cost porous carbon nanofibers (CNFs) using biomass tar, polyacrylonitrile (PAN), and silver nanoparticles has been demonstrated through electrospinning and subsequent stabilization and carbonization processes. The continuous electrospun nanofibers had average diameters ranging from 392 to 903 nm. The addition of biomass tar resulted in increased fiber diameters, reduced thermal stabilities, and slowed cyclization reactions of PAN in the as-spun nanofibers. After stabilization and carbonization, the resultant CNFs showed more uniformly sized and reduced average diameters (226−507 nm) compared to as-spun nanofibers. The CNFs exhibited high specific surface area (>400 m^2/g) and microporosity, attributed to the combined effects of phase separations of the tar and PAN and thermal decompositions of tar components. These pore characteristics increased the exposures and contacts of silver nanoparticles to the bacteria including Gram-positive *Staphylococcus aureus* and Gram-negative *Escherichia coli*, leading to excellent antimicrobial performances of as-spun nanofibers and CNFs. A new strategy is thus provided for utilizing biomass tar as a low-cost precursor to prepare functional CNFs and reduce environmental pollutions associated with direct disposal of tar as an industrial waste.

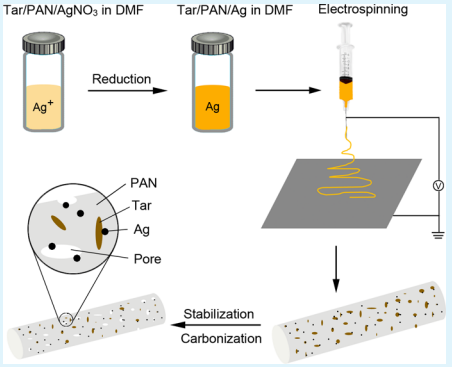

KEYWORDS: *biomass tar, carbon nanofibers, electrospinning, polyacrylonitrile, antimicrobial*

1. INTRODUCTION

Carbon nanofibers (CNFs) with diameters in the submicron and nanometer range have attracted increasing attention due to their superior chemical, electrical, and mechanical properties.[1−3] Among various CNFs, porous CNFs exhibit promising applications in energy conversion and storage, gas adsorption, and biomedical fields, attributed to their ultrahigh specific surface area and porosity.[4−6] The future demand for porous CNFs with diverse functionalities is expected to increase significantly and alternative raw materials have to be identified and implemented to reduce their production cost. Renewable raw materials from biomass sources are attractive for producing low-cost CNFs with minimal environmental impact due to their unique characteristics, including abundance and renewability.[7,8]

Tar, an industrial byproduct from biomass pyrolysis and gasification, is a potential source for producing such low-cost CNFs.[9] When tar is separated from biomass syngas, it has to be disposed of in an environmentally safe manner. Currently, tar is treated as an industrial waste, and its disposal is extremely difficult and costly due to its complex chemical composition and high resistance to biodegradation. Current efforts focus on tar reforming processes using steam or catalysts,[10,11] but these treatments are quite complicated, costly, and time-consuming. Our previous study indicated that biomass tar mainly contained phenols and aromatics originating from lignin decomposition during pyrolysis and gasification processes and presented with a high carbon content (i.e., >75%).[12] Thus, biomass tar can be a promising low-cost precursor for manufacturing CNFs. Tar or pitch derived from coal and petroleum was successfully processed into carbon fibers with a high specific surface area and porosity.[13,14] However, no reports of CNFs based on tar from biomass conversion have been found. It is thus of significant practical interest to utilize biomass tar as a low-cost precursor for carbon materials instead of disposing of it as a waste, causing environmental pollution.

CNFs are commonly produced through preparations of precursor fibers followed by thermo-oxidative stabilization and carbonization processes.[15] Although traditional spinning

Received: May 22, 2015
Accepted: June 25, 2015
Published: June 25, 2015

DOI: 10.1021/acsami.5b04479
ACS Appl. Mater. Interfaces 2015, 7, 15108−15116

methods, such as wet and melt spinning, have been used to manufacture precursor fibers, electrospinning emerges as a simple and highly versatile approach to fabricate multifunctional nanofibers with diameters down to a few nanometers.[16−19] Various polymeric materials, including polyacrylonitrile (PAN), cellulose, and pitch, are electrospun into precursor nanofibers, and diversified CNFs are obtained with subsequent stabilization, activation, and carbonization treatments.[1,20] The small dimension of electrospun CNFs creates a larger specific surface area compared to CNFs from traditional spinning methods.[21] Nevertheless, technical difficulties emerge from complex compositions of tar when it is used for electrospinning. Tar is composed of a number of mixed substances that cannot be completely dissolved by solvents. Furthermore, most components of tar have relatively low molecular weights. Thus, precursor suspensions prepared by tar exhibit inadequate homogeneity and low viscosity, which is detrimental for producing smooth and continuous electrospun fibers. Consequently, it is hard to obtain tar-based electrospun nanofibers with uniform diameters, and beaded or dumbbell shaped fibers were usually produced.[22,23] However, the electrospinning ability of tar can be improved by blending it with a polymer such as PAN with excellent electrospinning ability. The mixture of petroleum-derived pitch and PAN was successfully electrospun into continuous fibers, and activated carbon fibers with a high specific surface area ranging from 732 to 1877 m^2/g were prepared through subsequent stabilization, carbonization, and steam activation processes.[24] It is noteworthy that tar-derived CNFs may not be able to perform well in high strength applications due to the structural heterogeneity of tar, and efforts have been made to enhance their mechanical properties by modifying the compositions and molecular structures of the tar.[25] Nevertheless, tar can be used to fabricate electrospun CNFs with various functionalities, such as antimicrobial capacity, by incorporating silver nanoparticles.[26]

The aim of this study was to fabricate porous CNFs with antimicrobial capabilities from recycled biomass tar as a low-cost precursor by electrospinning and subsequent stabilization and carbonization processes. Suspensions of biomass tar, PAN, and silver nanoparticles were prepared and electrospun into precursor nanofibers that were further converted to porous CNFs by oxidative stabilization and carbonization in an inert atmosphere. The effects of tar loading levels on electrospinning ability of suspensions, morphologies, chemical structures, thermal properties, pore features, and antimicrobial performance of the resultant CNFs were investigated.

2. EXPERIMENTAL SECTION

2.1. Materials. Tar was collected from the gasification of corn stover at 500−600 °C from the Xigou Biomass Fuel Gas Plant in Shanxi, China. Its basic composition and properties were described in our previous report.[12] Water in the tar was removed by drying in a vacuum oven at 80 °C for at least 48 h. The dried tar was then stored in a sealed container for further processing. PAN (M_w = 150000 g/mol), *N*,*N*-dimethylformamide (DMF), and silver nitrate ($AgNO_3$) were purchased from Sigma-Aldrich (St. Louis, MO, USA).

2.2. Fabrication of Carbon Fiber Precursors. PAN was added in DMF and mixed using a magnetic stirrer for 24 h at room temperature. A certain amount of dried tar powder was dispersed in DMF under vigorous magnetic stirring for at least 24 h at room temperature. The PAN solution and tar suspension in DMF were blended, and the mixture was transferred to an ultrasonic bath to further disperse the tar in the blend for 30 min. The concentration of PAN in the mixture was fixed at 10 wt %. The loading levels of tar were 0, 50, and 100 wt % with respect to the weight of PAN (Table 1). Silver nitrate powder was then added to the prepared tar/PAN suspensions (molar ratio of $AgNO_3$ and repeating unit of PAN was 1/10). The resultant suspensions were shielded from light and stirred for 2 h in an ice bath to ensure complete dissolution of silver nitrate. Afterward, silver ions were reduced to silver nanoparticles by heating the suspensions to 90 °C in a water bath and holding at this temperature for 15 min. Finally, the suspensions containing tar, PAN, and silver nanoparticles were cooled to room temperature prior to electrospinning.

Table 1. Compositions and Carbon Yields of PAN/Ag and Tar/PAN/Ag Electrospun Nanofibers[a]

sample	C_{PAN} (wt %)	C_{tar} (wt %)	RSP	carbon yield
PAN/Ag	10	0	1/10	45
50Tar/PAN/Ag	10	50	1/10	44
100Tar/PAN/Ag	10	100	1/10	42

[a] C_{PAN} is the concentration of PAN in the suspensions. C_{Tar} is the content of tar based on the weight of PAN. RSP is the molar ratio of silver nitrate to the repeating unit of PAN. Carbon yield is based on the weight ratio of carbonized nanofibers to as-spun nanofibers.

Subsequently, each precursor suspension was loaded into a 5 mL BD plastic syringe attached to a stainless steel needle tip (internal diameter 0.584 mm). The needle was connected to a high-voltage power supply (Gamma High Voltage Research, Ormond Beach, FL, USA), which generated a positive DC voltage of 15 kV. The flow rate of the suspensions was controlled at 0.5 mL/h by an electric syringe pump (Chemyx Fusion 100, Stafford, TX, USA). A grounded metal plate covered with aluminum foil served as the collector, which was horizontally placed and perpendicular to the needle tip with a 20 cm separation. The collected nanofibers were dried in a vacuum oven to remove the residual solvent and stored in a desiccator prior to further treatments. The as-spun nanofibers were designated as PAN/Ag, 50Tar/PAN/Ag, and 100Tar/PAN/Ag with tar contents of 0, 50, and 100 wt % based on PAN by weight, respectively.

2.3. Stabilization and Carbonization. The following stabilization and carbonization were performed in a high temperature tubular furnace (GSL-1100, MTI Corporation, Richmond, CA, USA). The as-spun nanofibers were stabilized in air by heating up to 300 °C at a heating rate of 1 °C/min and holding at this temperature for 1 h. The stabilized nanofibers were subsequently carbonized in N_2 atmosphere by heating up to 900 °C at a heating rate of 5 °C/min and holding at this temperature for 1 h. The resultant CNFs are designated PAN/Ag-CNF, 50Tar/PAN/Ag-CNF, and 100Tar/PAN/Ag-CNF.

2.4. Characterization. Shear viscosities of the precursor suspensions were measured using a rheometer with a 40 mm cone−plate geometry (AR2000ex, TA Instruments, New Castle, DE, USA). The apparent viscosities were recorded at shear rates ranging from 0.1 to 1000 s^{-1} for each suspension at a controlled temperature of 25 °C using a Peltier device. A solvent trap cover was used to avoid solvent evaporation during the measurements. UV−vis measurements were performed to confirm Ag nanoparticle formation with a Varian UV−vis spectrophotometer (Evolution 600, Thermo Electron Corp., USA). The UV absorbance was collected at a wavelength range of 300−600 cm^{-1} for the electrospun suspensions diluted with the solvent (DMF).

Surface morphologies of the as-spun nanofibers and CNFs were examined by a field emission scanning electron microscope (FE-SEM, FEI QuantaTM 3D FEG Dual Beam SEM/FIB, Hillsboro, OR, USA) operated at 10 kV. The as-spun nanofibers were coated with a thin layer of gold prior to FE-SEM observation, and the CNFs were observed without coating. The diameters of the as-spun nanofibers and CNFs were obtained by measuring the randomly selected nanofibers on the FE-SEM images using image processing software (ImageJ 1.48). Fifty individual nanofibers were measured for each sample to determine the average diameter. The chemical structure information on the as-spun, stabilized, and carbonized nanofibers was obtained from a Bruker FTIR spectrometer (Alpha, Bruker Optics Inc., Billerica,

DOI: 10.1021/acsami.5b04479
ACS Appl. Mater. Interfaces 2015, 7, 15108−15116

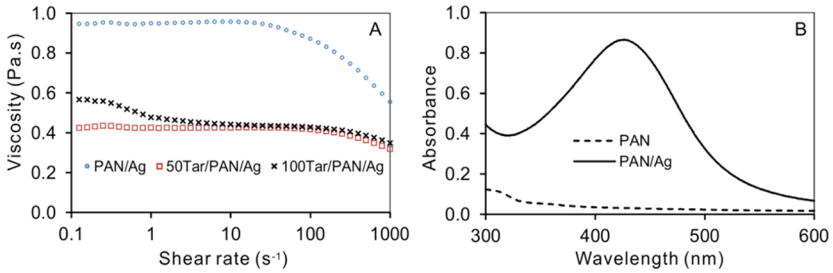

Figure 1. Basic properties of the electrospinning suspensions. (A) The shear viscosity-shear rate relationships for PAN/Ag, 50Tar/PAN/Ag, and 100Tar/PAN/Ag; (B) UV absorbance of PAN and PAN/Ag.

MA, USA) with an attenuated total reflectance (ATR) mode. The spectra were recorded between 4000 and 600 cm^{-1} with a spectral resolution of 4 cm^{-1}.

Thermal degradation of the as-spun and stabilized nanofibers was studied with a TA Q50 analyzer (New Castle, DE, USA) at a resolution of 0.1 μg. The thermogravimetric (TG) and differential thermogravimetric (DTG) curves were collected from 30 to 600 °C for the as-spun nanofibers and from 30 to 800 °C for the stabilized nanofibers at a heating rate of 10 °C/min. Sample weight was ~5.0 mg, and the test was conducted in a N_2 atmosphere with a N_2 flow rate of 60 mL/min. Differential scanning calorimetry (DSC) measurements were performed with a TA Q200 system in a nitrogen atmosphere with a nitrogen flow rate of 60 mL/min. Each sample with a weight of ~5 mg was scanned from 40 to 350 °C at a heating rate of 10 °C/min.

N_2 adsorption and desorption isotherms of the as-spun and CNFs were measured at 77 K on a Micromeritics TriStar II 3020 analyzer (Norcross, GA, USA). The samples were outgassed at 110 °C for 24 h in vacuum prior to data collection. The specific surface area and pore size distribution of the as-spun nanofibers were calculated using the Braunauer–Emmett–Teller (BET) method and the Barrett–Joyner–Halenda (BJH) method. The specific surface area of the CNFs was calculated both by BET and Langmuir methods. Density function theory (DFT), assuming slit-shaped pores, was used to determine the pore size distribution of the CNFs. The total pore volumes of the as-spun nanofibers and CNFs were obtained from the nitrogen adsorbed at a relative pressure of 0.99.

2.5. Antimicrobial Test. Antimicrobial activities of the as-spun nanofibers and CNFs against both Gram-positive *Staphylococcus aureus* (*S. aureus*) and Gram-negative *Escherichia coli* (*E. coli*) bacteria were tested according to the modified Kirby–Bauer method.[27,28] *S. aureus and E. coli* were cultivated in sterilized tryptic soy broth and incubated overnight at 37 °C in a shaking incubator. After 24 h, different dilutions were made by successively adding 1 mL aliquots of culture to 9 mL broth solutions. In the same manner, five serial dilutions were made. The diluted culture of 0.2 mL was then uniformly spread on an agar plate. The as-spun nanofiber and CNF membranes were cut into rectangles of 10 × 5 mm^2, sterilized by UV irradiation for 30 min, and placed on the agar plates containing bacteria for cultivation in an incubator at 37 °C for 24 h. Finally, the inhibition zones were observed after 24 h to assess the antimicrobial capability of the as-spun nanofibers and CNFs.

3. RESULTS AND DISCUSSION

3.1. Properties of Electrospinning Suspension. A homogeneous precursor suspension is a key prerequisite for successfully producing smooth and continuous electrospun nanofibers. In this study, homogeneous suspensions consisting of biomass tar, PAN, and silver nanoparticles were obtained using DMF as solvent due to its outstanding solubilization power for PAN and good dispersing ability for biomass tar. The shear viscosities of the precursor suspensions at a shear rate range of 0.1–1000 s^{-1} are shown in Figure 1A. The suspension without tar (PAN/Ag) exhibited Newtonian fluid behavior without obvious viscosity variations at low shear rates. Then, the viscosity decreased at high shear rates, and a pseudoplastic behavior was observed due to gradual disentanglements of PAN chains by increased shear stress. The suspension of 50Tar/PAN/Ag showed a similar behavior, but its viscosity value decreased by nearly half compared to the suspension of PAN/Ag as a result of the disruption of PAN molecular chain–chain interactions by the tar. The 100Tar/PAN/Ag showed almost the same viscosities as the 50Tar/PAN/Ag at middle and high shear rates, but exhibited higher viscosities at low shear rates. The initial shear thinning behavior at low shear rates was caused by the higher concentration of tar in 100Tar/PAN/Ag. The disruption of chain entanglements by increasing tar content made PAN molecules much easier to align, leading to immediate pseudoplastic fluid behavior at low shear rates.

$AgNO_3$ was dissolved at a low temperature and then reduced to silver nanoparticles by direct heating. DMF and the polyphenols in the tar probably served as reducing agents.[29–31] This green method was applied to avoid the use of environmentally hazardous chemical reducing agents, such as $NaBH_4$ and dimethylhydrazine. To confirm the formation of silver nanoparticles, UV absorbance of the suspensions was measured (Figure 1B). The PAN/Ag suspension showed an intensive absorbance peak at ~420 nm, whereas no peak around this wavelength was observed for the pure PAN solution. This peak was the characteristic surface plasmon resonance (SPR) band of silver nanoparticles,[32,33] and its presence indicated the formation of silver nanoparticles by reducing $AgNO_3$ in the suspensions.

3.2. Surface Morphology. Continuous electrospun nanofibers without beads were produced from the precursor suspensions with different tar/PAN ratios (Figure 2). However, some bulges appeared and became more obvious with increased tar content in the as-spun nanofibers, especially for the 100Tar/PAN/Ag composition. The rough surface resulted from aggregations of tar at a higher concentration and phase separations between the tar and PAN when the solvent rapidly evaporated during the traveling of electrospinning jets toward the collector.[23] Further increase in the tar loading levels made the electrospinning much more difficult and impractical due to undesirable tar aggregations and formations of inhomogeneous electrospinning suspensions. The average diameter of the as-spun nanofibers increased with an increase in the tar content with the values of 392 ± 48, 613 ± 50, and 903 ± 137 nm for PAN/Ag, 50Tar/PAN/Ag, and 100Tar/PAN/Ag, respectively (Figure 3). The increasing trend of the average diameters of the as-spun nanofibers with increased tar contents was due to increased concentrations of solutes (tar and PAN) in the precursor suspensions and lower contents of the solvent (DMF). In addition, the diameter variations of the as-spun nanofibers became much larger (Figure 3), resulting from

DOI: 10.1021/acsami.5b04479
ACS Appl. Mater. Interfaces 2015, 7, 15108–15116

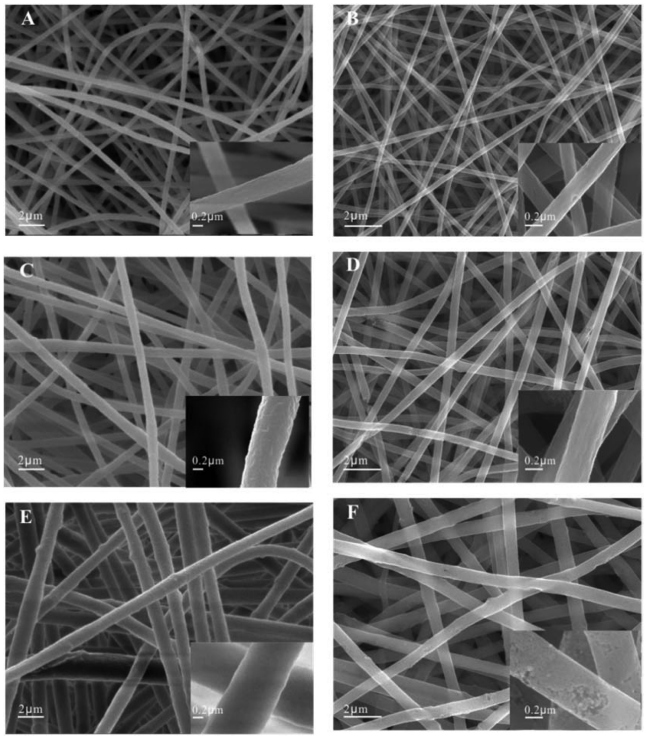

Figure 2. FE-SEM micrographs of the as-spun nanofibers with A: PAN/Ag, C: 50Tar/PAN/Ag, E: 100Tar/PAN/Ag) and CNFs (B: PAN/Ag-CNF, D: 50Tar/PAN/Ag-CNF, F: 100Tar/PAN/Ag-CNF (the inset at the bottom-right of each micrograph shows a higher magnification image).

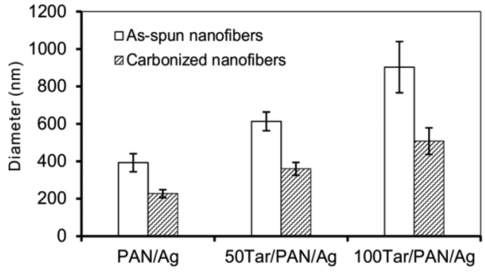

Figure 3. A comparison of average diameters of the as-spun nanofibers and CNFs from three different formulations.

rougher surfaces and more nonuniformly sized nanofibers with increased tar addition.

After the as-spun nanofibers were converted to CNFs by stabilization and carbonization, the continuous fibrous morphology was preserved (Figure 2). Compared with as-spun nanofibers, the average diameters of the CNFs decreased to 226 ± 21, 359 ± 34, and 507 ± 71 nm for PAN/Ag-CNF, 50Tar/PAN/Ag-CNF, and 100Tar/PAN/Ag-CNF, respectively (Figure 3). The resultant CNFs became more uniformly sized with smaller diameter variations compared to the as-spun nanofibers. This was caused by thermal decompositions and shrinkages of the as-spun nanofibers in the stabilization and carbonization processes. The thermal decompositions (mainly of tar components) also created more pores on the surfaces of the CNFs, especially for 100Tar/PAN/Ag-CNF (inset of Figure 2F).

3.3. Chemical Structure. ATR-FTIR spectra of the as-spun nanofibers are shown in Figure 4A. The distinctive absorbance features for PAN were present in all of the as-spun nanofibers, including C≡N stretching at 2245 cm^{-1}, CH_2 bending at 1452 cm^{-1}, CH wagging at 1256 cm^{-1}, and skeletal vibration of the PAN molecular chain at 1072 cm^{-1}.[34−36] Compared with PAN/Ag, the 50Tar/PAN/Ag and 100Tar/PAN/Ag compositions exhibited additional absorption peaks attributed to the main tar components (i.e., phenols, aromatics, acids, etc.), including 3300−3400 cm^{-1} (OH stretching), 1705 cm^{-1} (carbonyl stretching), 1609 cm^{-1} (aromatic skeletal vibration), and 830 and 764 cm^{-1} (C−H out-of-plane bending of aromatics).[12,23] These absorption peaks were not found in PAN/Ag without tar, indicating that the tar was successfully incorporated in the tar-containing as-spun nanofibers. In addition, the peaks at 2933 and 2871 cm^{-1} were ascribed to CH_2 stretching of both PAN and tar.

The chemical structure of the as-spun nanofibers was significantly altered by the oxidative stabilization treatment (Figure 4B). The most significant change was the decrease in the intensity of C≡N absorption at 2245 cm^{-1} for all the stabilized nanofibers. In addition, new absorption peaks at 1584 cm^{-1} attributed to the combination of C═N and C═C stretching, 1340 cm^{-1} ascribed to O−H bending (in-plane), and 806 cm^{-1} due to C═C−H bending were present.[37−39] These absorption peaks resulted from the generations of conjugated C═N containing structures from intramolecular cyclization of the nitrile groups and conjugated C═C structures from dehydrogenations at the stabilization stage.[15,38] In addition, the broad absorption band at 3100−3500 cm^{-1} was attributed to overlaps of the stretching bands from aromatic C−H, O−H, and N−H stretching in the stabilized nanofibers. Previous research also reported carbonyl groups at 1680 cm^{-1},[37,39] but this was not very obvious in the present study. These oxygen-containing groups (i.e., hydroxyl and carbonyl) were induced by the oxidative stabilization processes. The stabilized nanofibers were then subjected to thermal treatment in an inert atmosphere and thereby converted to the CNFs. Volatile compounds (e.g., HCN, H_2O, N_2, etc.) were removed to give the CNFs with a high carbon yield with respect to the original as-spun nanofibers. The FTIR spectra of the CNFs showed little discernible structure due to the strong absorbance of carbon (Figure 4C).

3.4. Thermal Properties. Thermal stability of the as-spun and stabilized nanofibers is shown in Figure 5. The PAN/Ag as-spun nanofibers, with no obvious weight loss up to 300 °C, underwent a fast decomposition stage from 300 to 350 °C (Figure 5A). However, the 50Tar/PAN/Ag and 100Tar/PAN/Ag as-spun nanofibers began to degrade at a much lower temperature than the PAN/Ag nanofibers due to lower initial degradation temperatures of tar components.[12] This was consistent with the DTG peaks of the as-spun nanofibers, which moved toward lower temperatures with increased tar contents. The residual weights of the PAN/Ag, 50Tar/PAN/Ag, and 100Tar/PAN/Ag as-spun nanofibers at 600 °C were 63, 58, and 49% of initial weights, respectively. The main decomposition temperatures of the stabilized nanofibers shifted to higher temperatures compared to the corresponding as-spun nanofibers, indicating the effectiveness of thermo-oxidative stabilization treatments. The weight loss of stabilized nanofibers was mainly due to the removal of volatile compounds by cross-linking condensation, dehydrogenation, and denitrogenation reactions.[15] In addition, the DTG peaks of the stabilized nanofibers at ∼180 °C were attributed to decompositions of the oxygen-containing groups, such as C═O and OH, in the stabilized nanofibers. Because of these thermal degradations,

DOI: 10.1021/acsami.5b04479
ACS Appl. Mater. Interfaces 2015, 7, 15108−15116

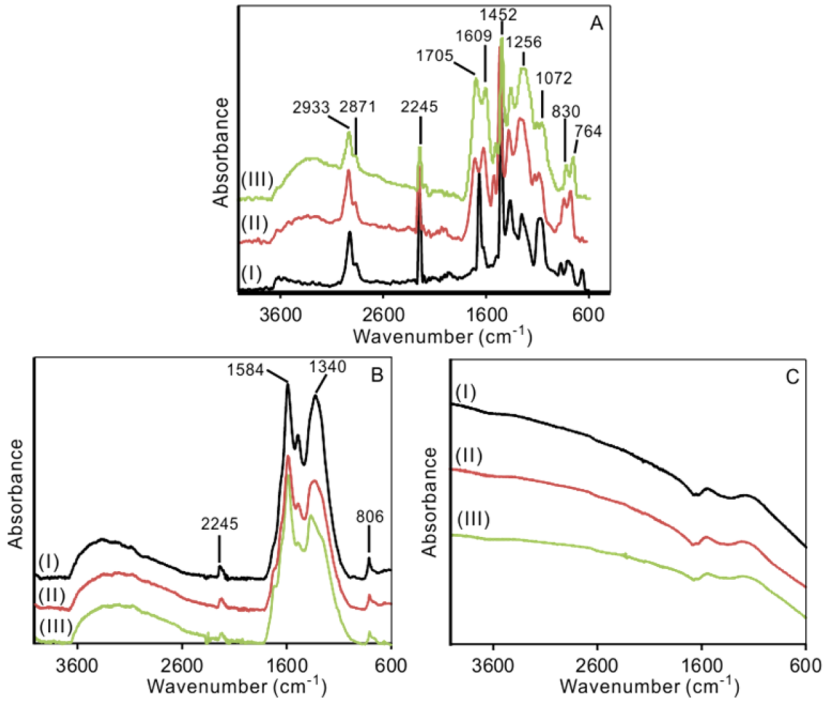

Figure 4. ATR-FTIR spectra of the as-spun (A), stabilized (B), and carbonized (C) nanofibers for different tar loading levels at I: PAN/Ag, II: 50Tar/PAN/Ag, and III: 100Tar/PAN/Ag.

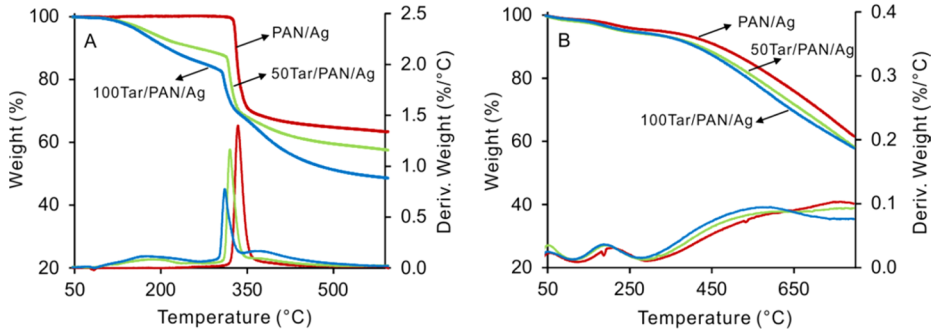

Figure 5. TG and DTG curves of the as-spun (A) and stabilized (B) nanofibers with three different tar contents.

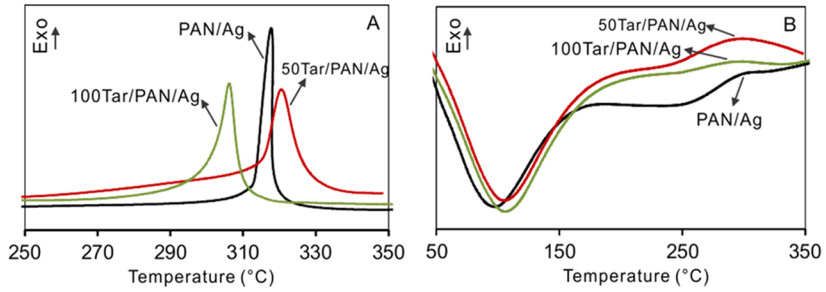

Figure 6. DSC curves of the as-spun (A) and stabilized (B) nanofibers with different tar contents.

the precursor nanofibers shrunk, and the formed CNFs exhibited reduced and more uniform diameters, confirming the morphological observations.

DSC curves of the as-spun PAN/Ag nanofibers showed a sharp exothermic peak at 317 °C (Figure 6A) attributed to the cyclization reactions of the nitrile groups in PAN.[15,37,40] Through the cyclization, the PAN polymer chains were converted to a heteroaromatic ladder structure. After the tar additions, the as-spun nanofibers exhibited a broader peak and initiated the cyclization reactions at lower temperatures. The peak temperature of 100Tar/PAN/Ag (305 °C) was much lower than that of PAN/Ag (317 °C), although there was no obvious difference between PAN/Ag and 50Tar/PAN/Ag (319 °C). These changes with tar additions indicated the change of the cyclization mechanism of PAN. It was recognized that the cyclization of PAN homopolymer initiated by a radical mechanism was faster than the cyclization of PAN copolymers following an ionic mechanism.[15,41] The ionizable groups of tar,

DOI: 10.1021/acsami.5b04479
ACS Appl. Mater. Interfaces 2015, 7, 15108−15116

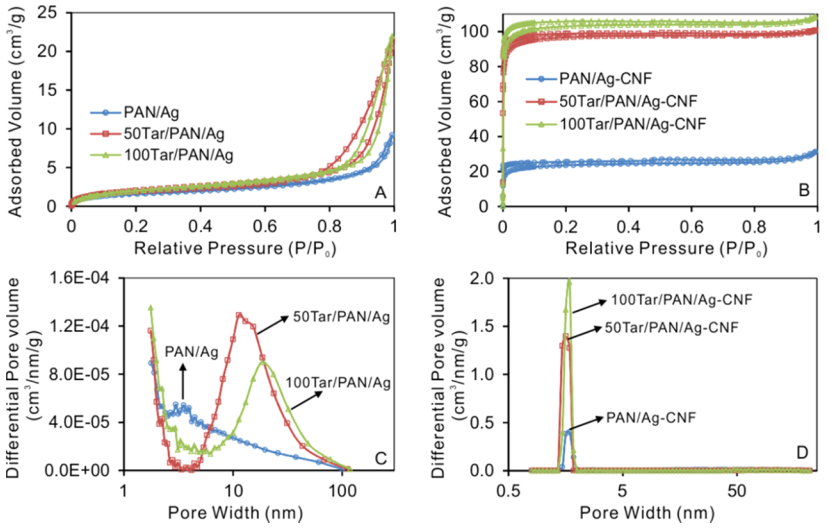

Figure 7. Pore characteristics of the as-spun nanofibers and CNFs with different tar contents, including (A) N_2 adsorption/desorption isotherms of the as-spun nanofibers at 77 K, (B) N_2 adsorption/desorption isotherms of the CNFs at 77 K, (C) pore size distributions of the as-spun nanofibers, and (D) pore size distributions of the CNFs.

such as hydroxyl and carboxylic groups located at the interfaces of PAN and tar, catalytically initiated the cyclization reactions of PAN and lowered the onset temperatures.[40] Although the tar slowed the cyclization reactions of PAN to avoid fusion of the as-spun nanofibers due to overheating by sharply exothermic reactions during subsequent thermal stabilization and carbonization, some structural flaws could be induced in the resultant CNFs by these ionic groups of tar, leading to inferior mechanical properties.[37] When the as-spun nanofibers were stabilized in air, the introduced oxygen-containing groups helped improve hygroscopicity of the stabilized nanofibers.[37,38] Thus, the endotherm peaks at 90−110 °C of the stabilized nanofibers were due to the release of water (Figure 6B). In addition, the PAN cyclization peaks of the stabilized nanofibers could barely be seen, indicating basic completion of the oxidative stabilization.

3.5. Pore Structure. N_2 adsorption/desorption isotherms and pore size distributions of the as-spun and CNFs are shown in Figure 7. According to the International Union of Pure and Applied Chemistry (IUPAC) classification,[42] the isotherms of the as-spun nanofibers were type IV with an H3 type hysteresis loop (Figure 7A), indicating the presence of mesopores (2 nm < pore size < 50 nm) in the nanofibers with a nonuniform size. This was consistent with the wide pore size distributions of the electrospun nanofibers determined by the BJH method (Figure 7C) with peak values of 3.5, 11.4, and 18.6 nm for PAN/Ag, 50Tar/PAN/Ag, and 100Tar/PAN/Ag, respectively. The BET specific surface area and total pore volume of the as-spun nanofibers also increased with an increase in the tar loading levels (Table 2). The increase in specific surface area, pore volume, and pore size with increased tar content in the as-spun nanofibers was attributed to phase separations of tar and PAN. The complex composition of tar made it extremely difficult blend well with PAN. Thus, phase separations between the tar and PAN during solvent evaporations contributed to the increase in surface area, volume, and pore size. This became more obvious when the tar components aggregated in some domains of the as-spun nanofibers.

During the stabilization and carbonization processes of the as-spun nanofibers, their pore structures underwent dramatic changes. Compared to the as-spun nanofibers, the CNFs had much higher specific surface area and pore volume (Table 2). On the basis of the IUPAC classification,[42] the isotherms of the CNFs are typical of type I (Figure 7B), indicating the dominance of micropores, which is similar to other PAN-based carbon fibers.[43] The N_2 adsorption completed at very low relative pressure regions (P/P_o < 0.05) because of multidirectional interactions between pore walls and the adsorbate. The pore size distribution calculated by DFT showed that the CNFs had a uniform pore size with peak values of 1.7, 1.6, and 1.7 nm for PAN/Ag-CNF, 50Tar/PAN/Ag-CNF, and 100Tar/PAN/Ag-CNF, respectively, confirming the predominance of micropores (Figure 7D). The tar-containing CNFs showed a much larger N_2 adsorption capacity compared to that of the CNFs without tar (Figure 7B). The specific surface area of the CNFs calculated by both BET and Langmuir methods indicated a large increase when the tar was added, and the pore volumes exhibited the same trend (Table 2), consistent with the FE-SEM observation. Furthermore, the fraction of micropore volumes for 50Tar/PAN/Ag-CNF (99.1%) and 100Tar/PAN/Ag-CNF (97%) was much higher than that for PAN/Ag-CNF (74.2%), similar to the results of pitch-based electrospun carbon fibers.[22] The large increase in the specific surface area and the high microporosity obtained with the tar incorporation was attributed to the combined effects of the two-phase

Table 2. Specific Surface Area and Pore Volume of the As-Spun Nanofibers and CNFs[a]

	S_{BET} (m^2/g)	$S_{Langmuir}$ (m^2/g)	V_p (cm^3/g)	V_{mp} (cm^3/g)	V_{mp}/V_p (%)
PAN/Ag	6.54		0.013	0.0009	6.9
50Tar/PAN/Ag	8.29		0.033	0.0006	1.8
100Tar/PAN/Ag	8.24		0.032	0.0005	1.6
PAN/Ag−CNF	94.79	97.78	0.043	0.0319	74.2
50Tar/PAN/Ag−CNF	410.25	414.38	0.133	0.1318	99.1
100Tar/PAN/Ag−CNF	437.81	439.50	0.144	0.1397	97.0

[a] S_{BET} is the BET specific surface area. $S_{Langmuir}$ is the specific surface area calculated by the Langmuir model. V_p is the total pore volume. V_{mp} is the micropore volume. V_{mp}/V_p is the fraction of micropore volume.

DOI: 10.1021/acsami.5b04479
ACS Appl. Mater. Interfaces 2015, 7, 15108−15116

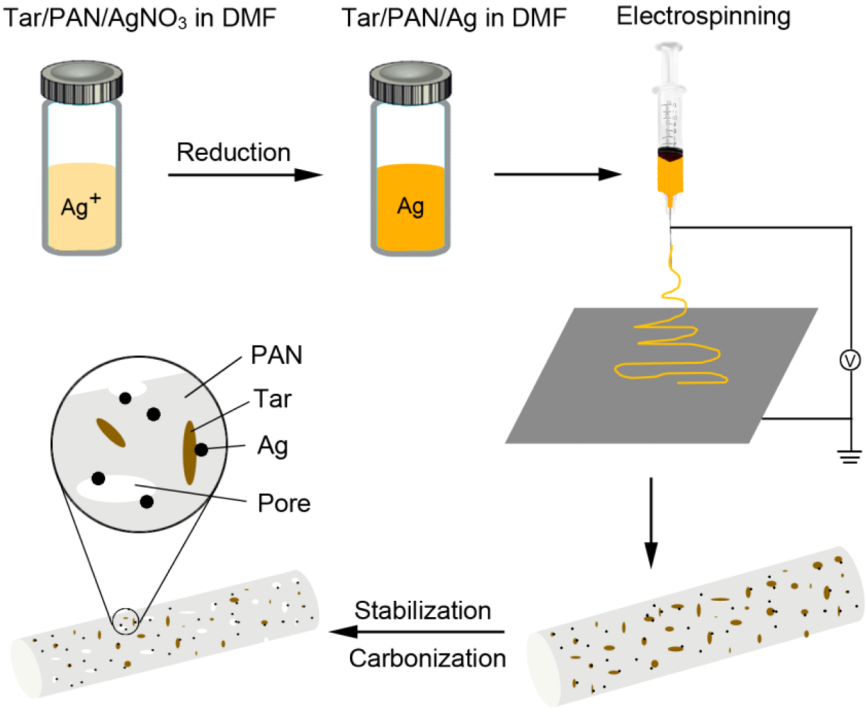

Figure 8. A schematic illustrating the fabrication of the porous tar-derived CNFs through electrospinning followed by stabilization and carbonization processes.

separations between the tar and PAN and thermal decompositions of the tar constituents. Similar results were reported in the PAN/pitch-derived electrospun CNFs.[44] The noticeably different structures of the tar and PAN caused inhomogeneous distributions of the tar in the PAN matrix and formation of tar aggregates throughout the as-spun nanofibers. Some aggregates of the tar degraded thermally when the as-spun nanofibers were converted to CNFs. Thus, more pores (mainly micropores) were created with tar addition, leading to increased specific surface area and larger micropore volumes in the CNFs (Figure 8).

3.6. Antimicrobial Performance. Formation of inhibition zones around the as-spun nanofibers and CNFs were monitored to evaluate their antimicrobial activities against *S. aureus* and *E. coli* (Figure 9 and Figure S1 in the Supporting Information). Clear inhibition zones around the as-spun nanofiber samples were observed after 24 h incubation, indicating their excellent antimicrobial efficiency against both *S. aureus* and *E. coli*. The antimicrobial activities were preserved after the stabilization and carbonization processes with obvious formation of inhibition zones around the CNFs. Silver nanoparticles, with their effective biocidal ability, were incorporated into the nanofibers to give antimicrobial capabilities, although the mechanism of killing microorganisms by silver was not clearly explained.[26,28,45] In this study, the silver nanoparticles were proposed to diffuse into the broth and to inhibit the growth of bacteria. The porous features of the as-spun nanofibers and CNFs resulted in large specific surface area and pore volume, which made the diffusion of silver nanoparticles into the broth easier, increasing the exposure and contact of silver nanoparticles to the bacteria (Figure 8).[28] Consequently, the tar-containing as-spun nanofibers and CNFs had higher specific surface area and pore volume, which might enhance their antimicrobial efficacy. The effect of tar loading levels on the antimicrobial performance of as-spun nanofibers and CNFs needs to be further studied. The antimicrobial efficacy was affected by the porosity and pore size distribution of the carbon materials, which could be controlled by tuning the composition and concentration of tar. Electrospun polymer nanofibers incorporated with silver nanoparticles were intensively studied and showed attractive applications in wound dressing, tissue scaffolds, and package materials.[46,47] The incorporation of tar could reduce the cost of silver-based antimicrobial materials.

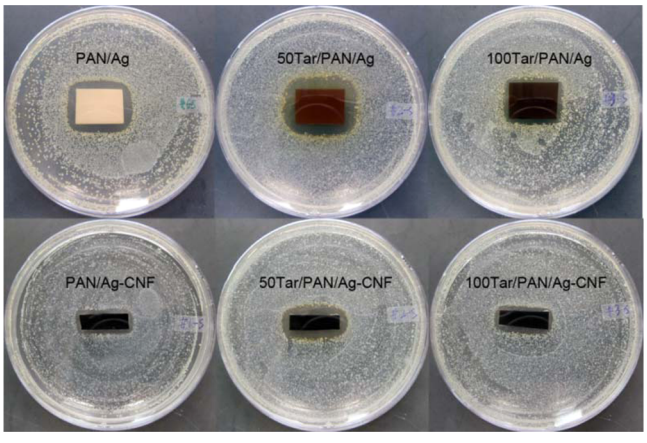

Figure 9. Antimicrobial activities of the as-spun nanofibers (upper row) and CNFs (lower row) with different tar contents against *S. aureus*.

4. CONCLUSION

Continuous microporous CNFs from biomass tar/PAN/silver hybrids with antimicrobial capabilities were fabricated through electrospinning and subsequent thermal stabilization and carbonization. Silver nitrate was reduced to silver nanoparticles,

DOI: 10.1021/acsami.5b04479
ACS Appl. Mater. Interfaces 2015, 7, 15108−15116

which conferred the antimicrobial abilities to the as-spun nanofibers and CNFs. The as-spun nanofibers showed larger average diameters with increased tar loading levels due to larger concentrations of tar and PAN in the suspensions. However, the increased contents of tar made the fiber surface rougher and increased fiber diameter variations resulted from tar aggregations and phase separations between tar and PAN. In addition, the incorporation of tar reduced the thermal stability of the as-spun nanofibers due to the relatively lower onset degradation temperatures of the tar components. The tar also slowed the cyclization reactions of PAN by its ionizable groups, which was helpful for subsequent stabilization processes. The as-spun nanofibers exhibited mesopore characteristics whereas micropores dominated in the CNFs due to the combined effects of thermal decompositions of some tar constituents and phase separations of tar and PAN. The large specific surface area and the volume of pores of the as-spun nanofibers and CNFs made the silver nanoparticles diffuse more easily into the broth, endowing their excellent antimicrobial abilities. Therefore, biomass tar can be a low-cost precursor for manufacturing antimicrobial carbon materials, extending applications of biomass products, and reducing environmental pollutions associated with tar disposal.

■ ASSOCIATED CONTENT

Supporting Information

The figure of antibacterial activities of the as-spun nanofibers and CNFs against *E. coli*. The Supporting Information is available free of charge on the ACS Publications website at DOI: 10.1021/acsami.5b04479.

■ AUTHOR INFORMATION

Corresponding Authors

*E-mail: wuqing@lsu.edu.
*E-mail: leitingzhou@163.com.

Notes

The authors declare no competing financial interest.

■ ACKNOWLEDGMENTS

The authors would like to gratefully acknowledge (i) financial support from the Economic Development Assistantship Program of Louisiana State University, (ii) Key Biomass Energy Laboratory of Henan Province in China for N_2 adsorption measurements, (iii) Dr. Chengjun Zhou for her technical help with electrospinning, (iv) Dr. Marlene Janes for her instructions concerning antimicrobial tests at LSU AgCenter Food Safety and Microbiology Lab, (v) Dr. Dongmei Cao for her technical help with FE-SEM observations, and (vi) Dr. Ioan I. Negulescu for his efforts with the USDA S-1041 project.

■ REFERENCES

(1) Zhang, L.; Aboagye, A.; Kelkar, A.; Lai, C.; Fong, H. A Review: Carbon Nanofibers from Electrospun Polyacrylonitrile and Their Applications. *J. Mater. Sci.* **2014**, *49*, 463−480.

(2) Morgan, P. *Carbon Fibers and Their Composites*, 1st ed.; Taylor & Francis Group: Boca Raton, FL, 2005.

(3) Gardea, F.; Naraghi, M.; Lagoudas, D. Effect of Thermal Interface on Heat Flow in Carbon Nanofiber Composites. *ACS Appl. Mater. Interfaces* **2014**, *6*, 1061−1072.

(4) Wang, M.; Huang, Z.; Bai, Y.; Kang, F.; Inagaki, M. Porous Carbon Nanofibers: Preparation and Potential Applications. *Curr. Org. Chem.* **2013**, *17*, 1434−1447.

(5) Xu, X.; Zhou, J.; Jiang, L.; Lubineau, G.; Chen, Y.; Wu, X. F.; Piere, R. Porous Core-shell Carbon Fibers Derived From Lignin and Cellulose Nanofibrils. *Mater. Lett.* **2013**, *109*, 175−178.

(6) Aykut, Y. Enhanced Field Electron Emission from Electrospun Co-loaded Activated Porous Carbon Nanofibers. *ACS Appl. Mater. Interfaces* **2012**, *4*, 3405−3415.

(7) Wu, Z.; Li, C.; Liang, H.; Chen, J.; Yu, S. Ultralight, Flexible, and Fire-resistant Carbon Nanofiber Aerogels from Bacterial Cellulose. *Angew. Chem.* **2013**, *125*, 2997−3001.

(8) Xu, X.; Zhou, J.; Jiang, L.; Lubineau, G.; Payne, S. A.; Gutschmidt, D. Lignin-based Carbon Fibers: Carbon Nanotube Decoration and Superior Thermal Stability. *Carbon* **2014**, *80*, 91−102.

(9) Song, K.; Wu, Q.; Zhang, Z.; Ren, S.; Lei, T.; Dooley, K. M.; Liu, D.; Janes, M. E. Fabricating Electrospun Nanofibers with Antimicrobial Capability: A Facile Route to Recycle Biomass Tar. *Fuel* **2015**, *150*, 123−130.

(10) Li, R.; Roy, A. D.; Bridges, J.; Dooley, K. M. Tar Reforming in Model Gasifier Effluents: Transition Metal/Rare Earth Oxide Catalysts. *Ind. Eng. Chem. Res.* **2014**, *53*, 7999−8011.

(11) Guan, G.; Kaewpanha, M.; Hao, X.; Zhu, A.; Kasai, Y.; Kakuta, S.; Kusakabe, K.; Abudula, A. Steam Reforming of Tar Derived from Lignin over Pompom-like Potassium-promoted Iron-based Catalysts Formed on Calcined Scallop Shell. *Bioresour. Technol.* **2013**, *139*, 280−284.

(12) Song, K.; Zhang, H.; Wu, Q.; Zhang, Z.; Zhou, C.; Zhang, Q.; Lei, T. Structure and Thermal Properties of Tar from Gasification of Agricultural Crop Residue. *J. Therm. Anal. Calorim.* **2015**, *119*, 27−35.

(13) Kim, B. J.; Kil, H.; Watanabe, N.; Seo, M. H.; Kim, B. H.; Yang, K. S.; Kato, O.; Miyawaki, J.; Mochida, I.; Yoon, S. H. Preparation of Novel Isotropic Pitch with High Softening Point and Solvent Solubility for Pitch-based Electrospun Carbon Nanofiber. *Curr. Org. Chem.* **2013**, *17*, 1463−1468.

(14) Derbyshire, F.; Andrews, R.; Jacques, D.; Jagtoyen, M.; Kimber, G.; Rantell, T. Synthesis of Isotropic Carbon Fibers and Activated Carbon Fibers from Pitch Precursors. *Fuel* **2001**, *80*, 345−356.

(15) Frank, E.; Steudle, L. M.; Ingildeev, D.; Spörl, J. M.; Buchmeiser, M. R. Carbon Fibers: Precursor Systems, Processing, Structure, and Properties. *Angew. Chem., Int. Ed.* **2014**, *53*, 5262−5298.

(16) Reneker, D. H.; Yarin, A. L. Electrospinning Jets and Polymer Nanofibers. *Polymer* **2008**, *49*, 2387−2425.

(17) Matsumoto, H.; Imaizumi, S.; Konosu, Y.; Ashizawa, M.; Minagawa, M.; Tanioka, A.; Lu, W.; Tour, J. M. Electrospun Composite Nanofiber Yarns Containing Oriented Graphene Nanoribbons. *ACS Appl. Mater. Interfaces* **2013**, *5*, 6225−6231.

(18) Zhou, J.; Gao, Q.; Fukawa, T.; Shirai, H.; Kimura, M. Macroporous Conductive Polymer Films Fabricated by Electrospun Nanofiber Templates and Their Electromechanical Properties. *Nanotechnology* **2011**, *22*, 275501.

(19) Zhou, J.; Li, E. Q.; Li, R.; Xu, X.; Ventura, I. A.; Moussawi, A.; Anjum, D. H.; Hedhili, M. N.; Smilgies, D.-M.; Lubineau, G. Semimetallic, Strong and Stretchable Wet-spun Conjugated Polymer Microfibers. *J. Mater. Chem. C* **2015**, *3*, 2528−2538.

(20) Joshi, P.; Zhang, L.; Chen, Q.; Galipeau, D.; Fong, H.; Qiao, Q. Electrospun Carbon Nanofibers as Low-cost Counter Electrode for Dye-sensitized Solar Cells. *ACS Appl. Mater. Interfaces* **2010**, *2*, 3572−3577.

(21) Inagaki, M.; Yang, Y.; Kang, F. Carbon Nanofibers Prepared via Electrospinning. *Adv. Mater.* **2012**, *24*, 2547−2566.

(22) Park, S. H.; Kim, C.; Choi, Y. O.; Yang, K. S. Preparations of Pitch-based CF/ACF Webs by Electrospinning. *Carbon* **2003**, *41*, 2655−2657.

(23) Park, S. H.; Kim, C.; Yang, K. S. Preparation of Carbonized Fiber Web from Electrospinning of Isotropic Pitch. *Synth. Met.* **2004**, *143*, 175−179.

(24) Bui, N. N.; Kim, B. H.; Yang, K. S.; Dela Cruz, M. E.; Ferraris, J. P. Activated Carbon Fibers from Electrospinning of Polyacrylonitrile/Pitch blends. *Carbon* **2009**, *47*, 2538−2539.

DOI: 10.1021/acsami.5b04479
ACS Appl. Mater. Interfaces 2015, 7, 15108−15116

(25) Kim, B. J.; Eom, Y.; Kato, O.; Miyawaki, J.; Kim, B. C.; Mochida, I.; Yoon, S. H. Preparation of Carbon Fibers with Excellent Mechanical Properties from Isotropic Pitches. *Carbon* **2014**, *77*, 747−755.
(26) Li, C.; Wan, Y.; Wang, J.; Wang, Y.; Jiang, X.; Han, L. Antibacterial Pitch-based Activated Carbon Fiber Supporting Silver. *Carbon* **1998**, *36*, 61−65.
(27) Rujitanaroj, P. o.; Pimpha, N.; Supaphol, P. Preparation, Characterization, and Antibacterial Properties of Electrospun Polyacrylonitrile Fibrous Membranes Containing Silver Nanoparticles. *J. Appl. Polym. Sci.* **2010**, *116*, 1967−1976.
(28) Kong, H.; Jang, J. Antibacterial Properties of Novel Poly(methyl methacrylate) Nanofiber Containing Silver Nanoparticles. *Langmuir* **2008**, *24*, 2051−2056.
(29) Wang, S.; Bai, J.; Li, C.; Zhang, J. Functionalization of Electrospun *β*-Cyclodextrin/Polyacrylonitrile (PAN) with Silver Nanoparticles: Broad-spectrum Antibacterial Property. *Appl. Surf. Sci.* **2012**, *261*, 499−503.
(30) Zou, M.; Du, M.; Zhu, H.; Xu, C.; Li, N.; Fu, Y. Synthesis of Silver Nanoparticles in Electrospun Polyacrylonitrile Nanofibers using Tea Polyphenols as the Reductant. *Polym. Eng. Sci.* **2013**, *53*, 1099−1108.
(31) Pastoriza-Santos, I.; Liz-Marzán, L. M. *N,N*-dimethylformamide as a Reaction Medium for Metal Nanoparticle Synthesis. *Adv. Funct. Mater.* **2009**, *19*, 679−688.
(32) Abdelgawad, A. M.; Hudson, S. M.; Rojas, O. J. Antimicrobial Wound Dressing Nanofiber Mats from Multicomponent (Chitosan/Silver-NPs/Polyvinyl Alcohol) Systems. *Carbohydr. Polym.* **2014**, *100*, 166−178.
(33) Li, Z.; Wang, L.; Chen, S.; Feng, C.; Chen, S.; Yin, N.; Yang, J.; Wang, H.; Xu, Y. Facilely Green Synthesis of Silver Nanoparticles into Bacterial Cellulose. *Cellulose* **2015**, *22*, 373−383.
(34) Liang, C. Y.; Krimm, S. Infrared Spectra of High Polymers. VII. Polyacrylonitrile. *J. Polym. Sci.* **1958**, *31*, 513−522.
(35) Arshad, S. N.; Naraghi, M.; Chasiotis, I. Strong Carbon Nanofibers from Electrospun Polyacrylonitrile. *Carbon* **2011**, *49*, 1710−1719.
(36) Kampalanonwat, P.; Supaphol, P. Preparation and Adsorption Behavior of Aminated Electrospun Polyacrylonitrile Nanofiber Mats for Heavy Metal Ion Removal. *ACS Appl. Mater. Interfaces* **2010**, *2*, 3619−3627.
(37) Wangxi, Z.; Jie, L.; Gang, W. Evolution of Structure and Properties of PAN Precursors During Their Conversion to Carbon Fibers. *Carbon* **2003**, *41*, 2805−2812.
(38) Wu, S.; Qin, X. Effects of the Stabilization Temperature on the Structure and Properties of Polyacrylonitrile-based Stabilized Electrospun Nanofiber Microyarns. *J. Therm. Anal. Calorim.* **2014**, *116*, 303−308.
(39) Dalton, S.; Heatley, F.; Budd, P. M. Thermal Stabilization of Polyacrylonitrile Fibres. *Polymer* **1999**, *40*, 5531−5543.
(40) Kim, J.; Kim, Y. C.; Ahn, W.; Kim, C. Y. Reaction Mechanisms of Polyacrylonitrile on Thermal Treatment. *Polym. Eng. Sci.* **1993**, *33*, 1452−1457.
(41) Gupta, A.; Paliwal, D.; Bajaj, P. Acrylic Precursors for Carbon Fibers. *J. Macromol. Sci. C* **1991**, *31*, 1−89.
(42) Sing, K.; Everett, D.; Haul, R.; Moscou, L.; Pierotti, R.; Rouquérol, J.; Siemieniewska, T. Reporting Physisorption Data for Gas/Solid Systems with Special Reference to the Determination of Surface Area and Porosity. *Pure Appl. Chem.* **1985**, *57*, 603−619.
(43) Park, S. J.; Jang, Y. S. Preparation and Characterization of Activated Carbon Fibers Supported with Silver Metal for Antibacterial Behavior. *J. Colloid Interface Sci.* **2003**, *261*, 238−243.
(44) Kim, B. H.; Yang, K. S.; Kim, Y. A.; Kim, Y. J.; An, B.; Oshida, K. Solvent-induced Porosity Control of Carbon Nanofiber Webs for Supercapacitor. *J. Power Sources* **2011**, *196*, 10496−10501.
(45) Song, J.; Kang, H.; Lee, C.; Hwang, S. H.; Jang, J. Aqueous Synthesis of Silver Nanoparticle Embedded Cationic Polymer Nanofibers and Their Antibacterial Activity. *ACS Appl. Mater. Interfaces* **2012**, *4*, 460−465.
(46) Rujitanaroj, P.-o.; Pimpha, N.; Supaphol, P. Wound-dressing Materials with Antibacterial Activity from Electrospun Gelatin Fiber Mats Containing Silver Nanoparticles. *Polymer* **2008**, *49*, 4723−4732.
(47) Xing, Z.; Chae, W.; Baek, J.; Choi, M.; Jung, Y.; Kang, I. In Vitro Assessment of Antibacterial Activity and Cytocompatibility of Silver-containing PHBV Nanofibrous Scaffolds for Tissue Engineering. *Biomacromolecules* **2010**, *11*, 1248−1253.

DOI: 10.1021/acsami.5b04479
ACS Appl. Mater. Interfaces 2015, 7, 15108−15116